TBK1 recruitment to STING activates both IRF3 and NF-κB that mediate immune defense against tumors and viral infections

Seoyun Yum[a,b,1], Minghao Li[a,b,1], Yan Fang[a,b], and Zhijian J. Chen[a,b,c,2]

[a]Department of Molecular Biology, University of Texas Southwestern Medical Center, Dallas, TX 75390-9148; [b]Center for Inflammation Research, University of Texas Southwestern Medical Center, Dallas, TX 75390-9148; and [c]HHMI, University of Texas Southwestern Medical Center, Dallas, TX 75390-9148

Contributed by Zhijian J. Chen, February 19, 2021 (sent for review January 5, 2021; reviewed by Katherine A. Fitzgerald and Akiko Iwasaki)

The induction of type I interferons through the transcription factor interferon regulatory factor 3 (IRF3) is considered a major outcome of stimulator of interferon genes (STING) activation that drives immune responses against DNA viruses and tumors. However, STING activation can also trigger other downstream pathways such as nuclear factor κB (NF-κB) signaling and autophagy, and the roles of interferon (IFN)-independent functions of STING in infectious diseases or cancer are not well understood. Here, we generated a STING mouse strain with a mutation (S365A) that disrupts IRF3 binding and therefore type I interferon induction but not NF-κB activation or autophagy induction. We also generated STING mice with mutations that disrupt the recruitment of TANK-binding kinase 1 (TBK1), which is important for both IRF3 and NF-κB activation but not autophagy induction (L373A or ΔCTT, which lacks the C-terminal tail). The STING-S365A mutant mice, but not L373A or ΔCTT mice, were still resistant to herpes simplex virus 1 (HSV-1) infections and mounted an antitumor response after cyclic guanosine monophosphate-adenosine monophosphate (cGAMP) treatment despite the absence of STING-induced interferons. These results demonstrate that STING can function independently of type I interferons and autophagy, and that TBK1 recruitment to STING is essential for antiviral and antitumor immunity.

cGAS | STING | interferon | TBK1 | NF-κB

Stimulator of interferon genes (STING) is an adaptor protein of the cytosolic DNA-sensing pathway that mediates immune responses against pathogens (1–3). Cytosolic DNA can arise from pathogen infections, cancer, or dysregulation of DNA clearance. The DNA-sensing enzyme cyclic guanosine monophosphate-adenosine monophosphate (GMP-AMP) synthase (cGAS) binds to DNA in the cytosol and produces cyclic GMP-AMP (cGAMP), the secondary messenger that binds to and activates STING (4, 5). cGAMP-bound STING traffics from the endoplasmic reticulum to the Golgi apparatus and drives the production of type I interferons (IFNs), expression of proinflammatory cytokines, and induction of autophagy (1–3, 6, 7). Activated STING recruits the downstream TANK-binding kinase 1 (TBK1) to the [(D or E)xPxPLR(S or T) D] motif (in which "x" denotes any amino acid) at the C-terminal tail (CTT) of STING (8). Activated STING proteins form large oligomers allowing the CTT-bound TBK1 to phosphorylate the CTT of neighboring STING proteins that are not bound to TBK1 (8). Among the phosphorylated residues at the CTT, serine 365 of mouse STING (equivalent to Ser366 in humans) within a sequence motif pLxIS (in which "p" denotes a hydrophilic residue) provides a binding site for interferon regulatory factor 3 (IRF3), thereby recruiting IRF3 for phosphorylation by nearby TBK1 (8–10). Phosphorylated IRF3 forms a dimer that translocates to the nucleus and induces type I IFNs and other cytokines. After activation by STING, TBK1 and its homolog IκB kinase epsilon (IKKε) can both lead to activation of the IKK complex, which then activates the transcription factor nuclear factor κB (NF-κB) (11, 12). NF-κB synergizes with IRF3 to induce high levels of type I IFN and other proinflammatory cytokines (13). In addition, STING trafficking induces noncanonical autophagy to clear DNA or pathogens from the cytosol (6).

The role of STING-induced type I IFNs has been extensively studied in infectious diseases and cancer, but the IFN-independent functions of STING in diseases are poorly understood. The core components of the cGAS-STING pathway are conserved from bacteria to humans (14–16), but only vertebrate STING contains the CTT that binds to TBK1 and IRF3 to induce IFNs. Nonvertebrate STING functions against pathogens without inducing type I IFNs: *Nematostella vectensis* STING induces autophagy (6) while *Drosophila melanogaster* STING induces autophagy and NF-κB activation (17, 18) to restrict viral infections.

Mice lacking cGAS or STING are highly susceptible to acute herpes simplex encephalitis (HSE) caused by herpes simplex virus (HSV) infection (19–21). Type I IFN signaling was suggested as the major mechanism of this antiviral effect as mice deficient in the interferon-α/β receptor (IFNAR) failed to clear viruses (22). However, the Toll-like receptor 3 (TLR3) pathway also induces IFNs in response to HSV-2 (23), and the direct role of STING-induced type I IFNs in antiviral responses in vivo has not been studied. In vitro, STING-induced autophagy was shown to be important for initially clearing HSV-1 from infected cells (6), suggesting that STING may trigger type I IFN-independent antiviral responses in addition to inducing IFN production.

Significance

The cGAS-STING pathway is important for immune defense against infection and cancer. STING activation triggers multiple signaling cascades leading to activation of IRF3, NF-κB, and autophagy. By generating mice harboring mutations of STING that specifically inactivate different signaling cascades, we found that ablation of IRF3 activation, which is essential for the induction of type I interferons, was not sufficient to abolish the immune defense against virus infection and cancer in mouse models. Rather, impairing the ability of STING to recruit TBK1, which is important for activating both IRF3 and NF-κB, abolished the immune defense functions of STING. These results demonstrate that the recruitment of TBK1 to STING has functions that are broader than activating IRF3 and inducing type I interferons.

Author contributions: S.Y., M.L., and Z.J.C. designed research; S.Y. and M.L. performed research; S.Y., M.L., and Y.F. contributed new reagents/analytic tools; S.Y., M.L., Y.F., and Z.J.C. analyzed data; and S.Y., M.L., and Z.J.C. wrote the paper.

Reviewers: K.A.F., University of Massachusetts Medical School; and A.I., Yale University.

The authors declare no competing interest.

[1]S.Y. and M.L. contributed equally to this work.

[2]To whom correspondence may be addressed. Email: zhijian.chen@utsouthwestern.edu.

This article contains supporting information online at https://www.pnas.org/lookup/suppl/doi:10.1073/pnas.2100225118/-/DCSupplemental.

Published March 30, 2021.

Tumor-derived DNA that accumulates in immune cells also activates the cGAS-STING pathway to promote cancer immune surveillance; STING was necessary to induce tumor-specific T cells and to control tumor growth (24). Activating cGAS or STING augmented antitumor immunity, providing a therapeutic effect in various tumor models (25). This antitumor effect was reduced in the absence of type I IFN signaling (26, 27), suggesting a critical role for IFNs in the STING-induced antitumor effect. However, the antitumor effects of other STING functions have not been well-characterized. During radiation-induced STING activation, the canonical NF-κB pathway enhanced the antitumor effect by promoting type I IFN expression whereas the noncanonical NF-κB pathway impeded the antitumor effect by reducing type I IFN expression (28). In addition to regulating IFN expression, NF-κB signaling not only induces inflammatory cytokines that promote immune cell functions but also provides an inflammatory tumor microenvironment that can promote tumor survival and metastasis (29).

In order to study the type I IFN-independent functions of STING in diseases, we generated three different STING mutant mouse strains that exhibited partial loss of STING functions: S365A, L373A, and C-terminal tail truncation (ΔCTT). Using these mouse models, we observed that STING-S365A mutant mice, which lack STING-induced IRF3 activation but retain NF-κB activation, were still resistant to HSV-1 infections and mount an antitumor response against the Lewis lung cancer model after cGAMP treatment. This antiviral and antitumor effect was not found in the L373A and ΔCTT mutants that were defective in recruiting TBK1 and therefore unable to activate IRF3 and NF-κB. Activation of the STING-S365A mutant stimulated immune cells and instigated NF-κB–induced immunostimulatory gene expression. Our study demonstrates the critical role of TBK1 recruitment by STING in antiviral and antitumor immunity and reveals a type I IFN-independent function of STING that is critical for understanding STING-related diseases. This result is in line with recent studies reporting the type I IFN-independent antiviral effect in STING-S365A mice (30, 31) and further defines the mechanism using STING-L373A mice.

Results

STING Mutant Mice with Distinct Signaling Defects. In order to determine the role of STING activation in different disease models, we generated three STING mutant mice using the CRISPR-Cas9 system (*SI Appendix*, Table S1). The S365A mutation is defective in phosphorylation, thereby disrupting recruitment of IRF3 while retaining the ability to recruit TBK1 (10). The L373A mutation disrupts the TBK1 recruitment motif and is defective in both IRF3 and NF-κB activation (8). The ΔCTT mutation has a stop codon after amino acid 339, thereby producing a truncated protein lacking the C-terminal tail (residues 340 to 378) that is important for TBK1 binding. All three mutants are expected to be capable of binding cGAMP and inducing autophagy (6). We isolated bone marrow-derived dendritic cells (BMDCs) and bone marrow-derived macrophages (BMDMs) from the STING mutant mice and stimulated the cells with the mouse STING agonist 5,6-dimethylxanthenone-4-acetic acid (DMXAA), which is more permeable to cells than cGAMP. Western blotting of the protein lysates from BMDCs (Fig. 1*A*) and BMDMs (*SI Appendix*, Fig. S1*A*) showed gradual loss of the downstream signaling pathways. All BMDCs expressed STING or its mutant proteins except the STING-Goldenticket ($Sting^{gt}$) mutant, which carries an I199N null mutation that renders the loss of STING expression (32). Notably, STING-S365A, but not STING-L373A, preserved the mobility shift of STING in the Western blot, indicating TBK1-mediated phosphorylation of other residues at the CTT as previously described (9, 10). All mutants lacked phosphorylation of the STING-S365 residue, IRF3, and STAT1 upon stimulation, indicating defects in IRF3 activation and type I IFN signaling (9) (Fig. 1*A* and *SI Appendix*, Fig. S1*A*). Consistently, all mutants were deficient in IRF3 nuclear translocation (Fig. 1*B* and *SI Appendix*, Fig. S1*B*) and did not produce IFNβ after DMXAA treatment (Fig. 1*C*). Despite the lack of IFN signaling, STING-S365A cells retained normal activation of TBK1 and IKKε, as shown by their phosphorylation. Phosphorylation of p65 and IκBα, indicating NF-κB signaling, was intact in the STING-S365A cells (Fig. 1*A* and *SI Appendix*, Fig. S1*A*). DMXAA-treated STING-L373A and -ΔCTT cells lacked IFN and NF-κB signaling as shown by the absence of phosphorylated STAT1, TBK1, IKKε, p65, and IκBα (Fig. 1*A* and *SI Appendix*, Fig. S1*A*). Consistent with the Western blotting data, p65 nuclear translocation was deficient in L373A and ΔCTT cells but not in S365A cells (Fig. 1*B* and *SI Appendix*, Fig. S1*B*). Autophagy induction, which is indicated by the conversion of microtubule-associated protein 1A/1B-light chain 3 (LC3) from LC3-I (upper band in longer exposure blot) to LC3-II (lower and darker band in normal and longer exposure blots), was intact in S365A and L373A cells (Fig. 1*A*). This is consistent with a previous study showing that deletion of the CTT from STING did not impair LC3 lipidation (6). However, the autophagy induction seems to be weaker in the STING-ΔCTT cells (Fig. 1*A*), which might be due to a lower level of expression in the STING-ΔCTT protein in BMDCs.

STING-S365A Mice, but Not -L373A or -ΔCTT Mice, Are Resistant to HSV-1 Infection. STING-deficient mice are susceptible to HSV-1 infection whereas wild-type (WT) mice survive and clear the virus within a few days (20). To determine which functions of STING led to this protection against HSV-1, we retroorbitally infected WT, $Ifnar1^{-/-}$, and different STING mutant mice and assayed their responses. $Ifnar1^{-/-}$ mice succumbed to the virus infection early on as previously reported (Fig. 2*A* and *SI Appendix*, Fig. S2*A*) (22). Production of serum IFNβ was confirmed 6 h after infection in WT and $Ifnar1^{-/-}$ mice but not in any of the STING mutant mice (Fig. 2*B*). However, lower levels of IFNβ were detected in the sera of WT and all STING mutant mice 2 d after infection, indicating that pathways other than STING can detect HSV-1 and produce IFNβ at a later time point (*SI Appendix*, Fig. S2*B*). Despite the lack of STING-induced IFNβ, STING-S365A mice were partially resistant to HSV-1 infection as indicated by their survival rate, body weight change, and viral titer in the brain being similar to those measurements from WT mice (Fig. 2 *A* and *C* and *SI Appendix*, Fig. S2*A*). In contrast, the mice harboring the L373A mutation and C-terminal deletion (ΔCTT) of STING all succumbed to HSV-1 infection and had high viral titers in the brain, similar to the STING-deficient mice ($Sting^{gt}$). These results indicate that TBK1 recruitment to STING, which is important for both IRF3 and NF-κB activation, is essential for immune defense against HSV-1. Because the STING-L373A mutant, and to a lesser extent the ΔCTT mutant, can still induce autophagy, the results also suggest that autophagy induction by STING alone is insufficient to protect the mice from HSV-1 infection in vivo.

All BMDCs harboring the STING mutations secreted markedly less (~1,000-fold reduction) but still detectable levels of IFNβ after HSV-1 infection (*SI Appendix*, Fig. S2*C*), indicating that STING is the main pathway producing IFNβ after initial infection although other pathways may still partially contribute. Furthermore, STING-induced type I IFN provided an immediate and direct antiviral effect in vitro; all IFN-deficient mutant BMDCs showed more green fluorescent protein-positive (GFP^+) cells after HSV-GFP infection (*SI Appendix*, Fig. S2*D*) and acquired higher viral genome equivalent (VGE) counts after HSV-1 infection (*SI Appendix*, Fig. S2*E*). Despite this antiviral effect in vitro, STING-induced IFN was dispensable for protecting the STING-S365A mice from HSV-1 infection (Fig. 2*A*).

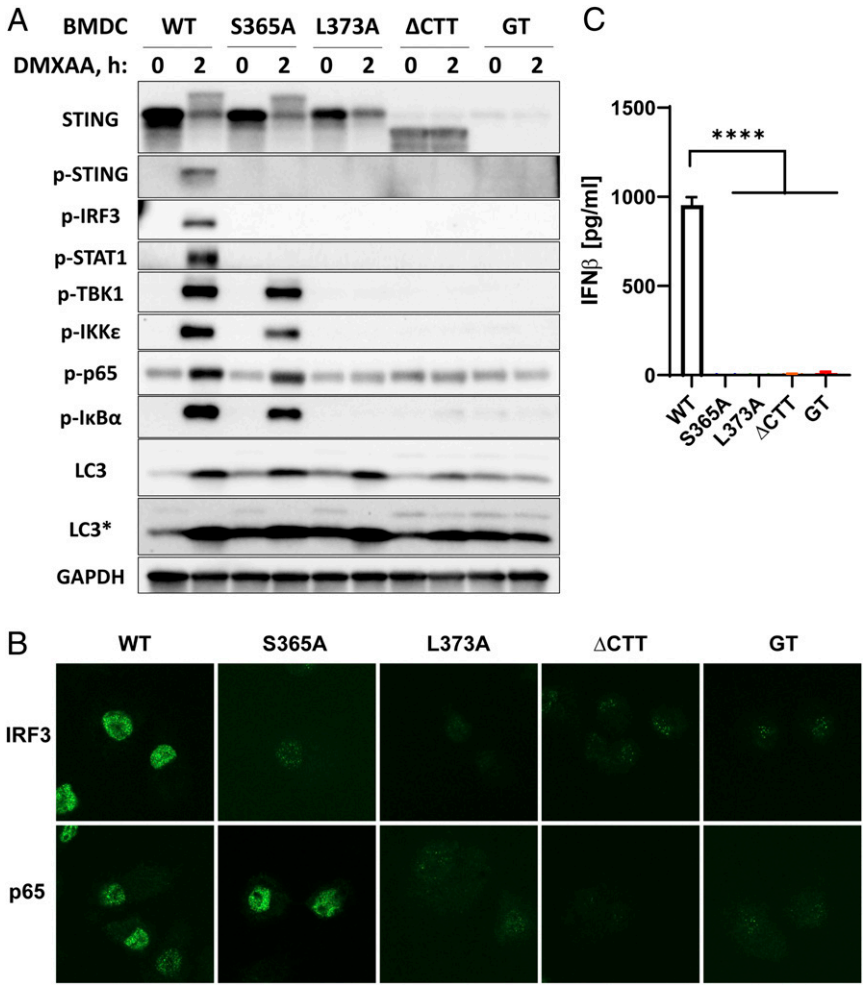

Fig. 1. STING mutants with distinct signaling defects. BMDCs were prepared from mice harboring the indicated mutations. (*A*) Western blots of crude lysates from BMDCs treated with 75 μM DMXAA for 2 h. Antibodies detect specific phosphorylated residues of proteins and are listed in *Materials and Methods*. LC3* indicates a longer exposure. (*B*) Immunofluorescence staining of IRF3 and p65 in BMDCs treated with 75 μM DMXAA for 1 h. (*C*) IFNβ levels measured by ELISA in the BMDM culture media 6 h after 75 μM DMXAA treatment. Error bars represent SEM. ****$P < 0.0001$. Results are representative of at least two independent experiments.

STING Activation Promotes a Type I IFN-Independent Antitumor Effect. The cGAS-STING pathway is an endogenous pathway that detects tumors and initiates immune responses (24); thus, host cGAS was required for the antitumor effect of the immune checkpoint inhibitor anti–PD-L1 in the B16 melanoma mouse model (33). Here, we used the Lewis lung carcinoma (LL2) tumor model to study the antitumor effect of STING activation in immunologically cold tumors. In order to confirm the spontaneous detection of the LL2 tumor by the immune system, we implanted LL2 tumors into IFNβ-luciferase reporter mice. IFNβ-luciferase reporter mice showed weak basal levels of luciferase signal without tumor implantation (*SI Appendix*, Fig. S3*A*), as was observed previously (34). However, a stronger IFNβ-driven luciferase signal was found at the tumor area in a cGAS-dependent manner (*SI Appendix*, Fig. S3 *A* and *B*), indicating the detection of the LL2 tumor by cGAS. As previously reported (35), the LL2 tumor was resistant to anti–PD-L1 therapy (*SI Appendix*, Fig. S3*C*) despite the induction of PD-L1 by IFNγ or IFNβ treatment (*SI Appendix*, Fig. S3*D*) and the expression of PD-L1 on the cell surface of tumor cells isolated from mice (*SI Appendix*, Fig. S3 *E* and *F*).

Despite the poor immunogenicity of the LL2 tumors, intratumoral cGAMP treatment reduced the LL2 tumor growth in a dose-dependent manner (Fig. 3*A*). Sting^{gt} mice completely lost this antitumor effect, indicating that the activation of host STING is essential for the antitumor effect of cGAMP (*SI Appendix*, Fig. S4*A*). LL2 tumor cells also have a functional STING pathway that induces TBK1 phosphorylation and CXCL10 expression upon activation (*SI Appendix*, Fig. S4 *C* and *D*). To determine the role of tumor STING in this cGAMP-induced antitumor response, we generated an LL2-STING$^{-/-}$ clonal cell line using CRISPR-Cas9 that abrogated STING downstream signaling (*SI Appendix*, Fig. S4 *C* and *D*). Consistent with this result, LL2-STING$^{-/-}$ cells implanted into Sting^{gt} mice also abrogated the residual interferon-stimulated gene (ISG) levels in the tumor after intratumoral cGAMP treatment (*SI Appendix*, Fig. S4*E*). WT mice implanted with this LL2-STING$^{-/-}$ cell line still showed a significant reduction in tumor size after cGAMP treatment while inducing ISGs in the tumor and draining lymph node, indicating that host STING is sufficient to mediate the antitumor effect of cGAMP (*SI Appendix*, Fig. S4 *B* and *E*).

We also treated LL2 tumors with cGAMP at later time points (days 9 and 13) and analyzed the tumor-infiltrating immune cells (*SI Appendix*, Fig. S5 *A*–*E*). The tumor weights were comparable 1 d after the last cGAMP treatment (*SI Appendix*, Fig. S5*A*), but the cGAMP-treated group showed more recruitment of CD45^{+}

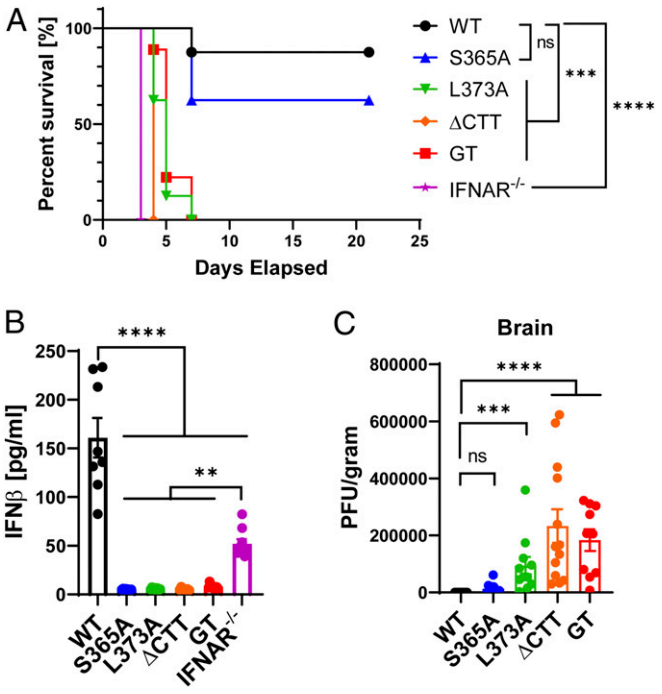

Fig. 2. STING-S365A mice, but not L373A or ΔCTT mice, are resistant to HSV-1 infection. (*A* and *B*) Mice ($n = 7$ to 9) were retroorbitally infected with HSV-1 (5×10^6 plaque-forming units per mouse). (*A*) Survival curve. (*B*) Serum IFNβ levels 6 h postinfection. (*C*) Mice ($n = 10$ to 13) were infected with HSV-1 (5×10^6 plaque-forming units [pfu] per mouse). The viral titer in the brain was measured by plaque assay 4 d postinfection. Error bars represent SEM. $^{**}P < 0.01$, $^{***}P < 0.001$, $^{****}P < 0.0001$; ns, not significant. Results are representative of at least two independent experiments.

cells into the tumor (*SI Appendix*, Fig. S5*B*). The percentage of $CD8^+$ T cells and natural killer (NK) cells did not increase, and the percentage of $CD4^+$ T cells decreased after cGAMP treatment (*SI Appendix*, Fig. S5*C*); however, all tumor-infiltrating lymphocytes up-regulated CD69, indicating their activation (*SI Appendix*, Fig. S5*D*). The most drastic change induced by cGAMP treatment in the tumor cell population was in cells from the myeloid lineage; the percentage of neutrophil-like cells increased while monocyte-like cells decreased (*SI Appendix*, Fig. S5*E*). Tumor-infiltrating neutrophils have both antitumor (N1) and protumor (N2) functions (36). cGAMP treatment, along with inducing IFNβ, CXCL10, and IFNγ, also up-regulated nitric oxide synthase 2 (NOS2) and down-regulated arginase 1 (ARG1) in the tumor, which suggests polarization toward the N1 phenotype (*SI Appendix*, Fig. S5*F*). We then depleted $CD8^+$ T cells and NK cells in the tumor-implanted mice and confirmed the depletion in the spleen until end point (*SI Appendix*, Fig. S5*G*). Depleting NK cells (*SI Appendix*, Fig. S5*H*), but not $CD8^+$ T cells (*SI Appendix*, Fig. S5*I*), partially reduced the antitumor effect of cGAMP.

Type I IFN signaling is essential for the therapeutic effect of cGAMP in various tumor models (26, 27). For the LL2 tumor model, cGAMP treatment showed a weaker but still significant reduction in tumor volume for *Ifnar1*$^{-/-}$ mice (Fig. 3*B*). As type I IFN may act on the LL2 cells, we injected anti–IFNAR-1 antibodies into *Ifnar1*$^{-/-}$ mice tumors to further block type I IFN signaling. cGAMP still exerted a significant antitumor effect even with this treatment (*SI Appendix*, Fig. S6*A*), which further reduced the ISG levels in the tumor and spleen (*SI Appendix*, Fig. S6*B*). These results demonstrate that cGAMP exerts both type I IFN-dependent and -independent antitumor effects.

Next, we tested the effect of cGAMP treatment on LL2 tumors in STING mutant mice to study the role of the downstream signaling pathways. cGAMP treatment reduced tumor sizes only in WT and STING-S365A mice but not in -L373A or -ΔCTT mice (Fig. 3*C*), even though all STING mutant mice lacked serum IFNβ production in response to intratumoral cGAMP treatment (Fig. 3*D*). Our data demonstrate that intratumoral cGAMP treatment exerts a therapeutic effect on LL2 tumors by activating host STING, which triggers both type I IFN-dependent and type I IFN-independent antitumor effects. Autophagy is not sufficient to drive antitumor immunity as STING-L373A mice lost the antitumor response. STING-S365A mice retained NF-κB activation, which may provide an immunostimulatory effect and compensate for the loss of IFN signaling.

Transcriptome Analysis of STING-Induced Type I IFN-Independent Genes. In order to identify the IFN-independent functions of STING that mediate the antiviral and antitumor effect, we performed a transcriptome analysis of STING mutant BMDMs stimulated with DMXAA. WT cells induced a large number of genes including IFNβ, ISGs, and other cytokines (*SI Appendix*, Fig. S7*A*). Some of these genes were expressed at lower levels in STING-S365A mutant cells but not in L373A, ΔCTT, or Sting^{gt} cells. Interestingly, DMXAA-treated S365A BMDMs also induced expression of several genes at levels higher than even WT cells did (*SI Appendix*, Fig. S7*A*). Kyoto Encyclopedia of Genes and Genomes (KEGG) pathway analysis of the transcriptome data shows the activation of cytokine signaling pathways in S365A mutant cells; specifically, genes in the NF-κB signaling pathway were more enriched in the S365A cells than in the WT cells (*SI Appendix*, Fig. S7*B*). The top 20 up-regulated genes in the S365A cells included NF-κB–induced genes such as Cxcl1, Cxcl2, Tnfsf9 (4-1BBL), and Ptgs2 (COX2) (Fig. 4*A*). qRT-PCR analysis of stimulated BMDCs and BMDMs confirmed the expression of these genes (Fig. 4 *B*–*D* and *SI Appendix*, Fig. S8). None of the STING mutant cells induced IFNα, IFNβ, or ISGs (Fig. 4 *B* and *C* and *SI Appendix*, Fig. S8*A*); STING-S365A cells, however, expressed CXCL1, CXCL2, 4-1BBL, and COX2 at higher levels than even WT cells did (Fig. 4*D* and *SI Appendix*, Fig. S8*B*). It is possible that these NF-κB–regulated genes are more highly expressed in the absence of activated IRF3.

In cGAMP-treated tumors, IFNβ production was the highest 4 h after cGAMP injection as shown by the tumor luciferase activity in the IFNβ-luciferase reporter mice (*SI Appendix*, Fig. S9*A*). At this time point, cGAMP-treated WT mice, but not any STING mutant mice, expressed ISGs and IFNγ in the spleen (*SI Appendix*, Fig. S9*B*). As tumor STING is functional, tumors from STING mutant mice still induced low levels of IFNβ and ISGs after cGAMP treatment; this expression level, however, was significantly lower than those in the tumors of the WT mice (*SI Appendix*, Fig. S9*C*). Tumors from WT and S365A mutant mice, but not from other mutants, expressed NF-κB–induced genes such as CXCL1 and CXCL2 after cGAMP treatment. Tumor necrosis factor α (TNFα) and interleukin-1β (IL-1β), which are regulated by both IRF3 and NF-κB, were down-regulated in the tumors of all STING mutant mice (*SI Appendix*, Fig. S9*C*), likely due to the lack of IRF3 activation. These up-regulated NF-κB–induced genes may play a role in activating innate and adaptive immune cells, providing an immunostimulatory effect for antitumor immunity.

Type I IFN-Independent Functions of STING Have Immunostimulatory Effects. To investigate whether the type I IFN-independent functions of STING have immunostimulatory effects, we analyzed the activation markers of STING mutant immune cells upon stimulation. WT and STING-S365A BMDCs, but not BMDCs from other STING mutants, up-regulated major histocompatibility complex class II (MHC-II) and the costimulatory molecules CD86, CD80, and CD40 after DMXAA treatment (Fig. 5*A*). Similar to WT cells,

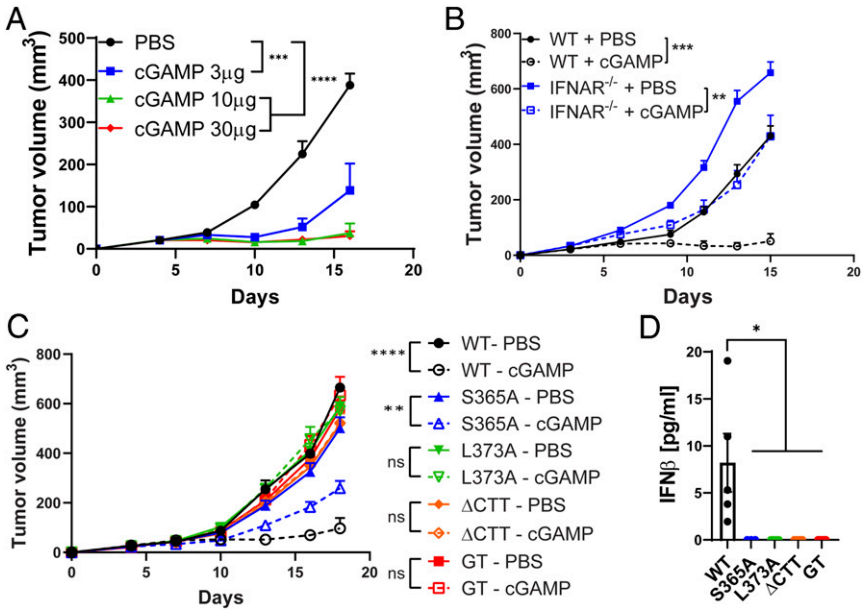

Fig. 3. cGAMP exerts an antitumor effect in STING-S365A mice but not in L373A or ΔCTT mice. (*A*–*C*) LL2 tumor growth after intratumoral cGAMP treatments. (*A*) WT mice ($n = 5$) were treated with the indicated doses of cGAMP on days 4, 7, and 10 after LL2 implantation. (*B*) WT and *Ifnar1*$^{-/-}$ mice ($n = 4$ to 6) were treated with 10 μg of cGAMP on days 3, 6, and 9 after LL2 implantation. (*C*) Mice ($n = 4$ to 8) were treated with 10 μg of cGAMP on days 5, 8, 11, and 14 after LL2 implantation. (*D*) Serum IFNβ levels 6 h postintratumoral cGAMP treatment. cGAMP (10 μg) was injected on days 7 and 9 after tumor implantation; serum was collected 6 h after the last cGAMP injection. Error bars represent SEM. *$P < 0.05$, **$P < 0.01$, ***$P < 0.001$, ****$P < 0.0001$. Results are representative of at least two independent experiments.

STING-S365A splenocytes stimulated with DMXAA up-regulated CD69 on CD4$^+$ and CD8$^+$ T cells, B cells, and NK cells, although the CD69 expression level was lower in CD4$^+$ T cells from S365A mice than in those from WT mice (Fig. 5*B*). In contrast, DMXAA-induced up-regulation of CD69 was abolished in all cells from L373A, ΔCTT, and Sting^{gt} mice (Fig. 5*B*).

We then immunized the STING mutant mice with the model antigen ovalbumin (OVA) with cGAMP. After prime-boost immunization, cGAMP-treated WT mice displayed higher levels of serum anti-OVA immunoglobulin G (IgG) compared with the WT mice treated only with OVA (Fig. 5*C*). This adjuvant effect of cGAMP was retained in STING-S365A mice, albeit at a lower level, and was abrogated in L373A, ΔCTT, and Sting^{gt} mice (Fig. 5*C*). However, OVA and cGAMP immunization did not increase OVA-specific CD8$^+$ T cell populations (Fig. 5*D*). T cell activation by IFN-independent functions of STING in vitro (Fig. 5*B*), but not in vivo (Fig. 5*D*), suggests that stronger stimulation or activation of T cell STING may be needed for T cell activation in vivo. Altogether, these data demonstrate that STING can activate innate and adaptive immune cells in vitro and elicit significant antibody responses in a manner that depends on TBK1 recruitment but not type I IFNs.

Discussion

Prior studies on antiviral and antitumor immunity revealed that the cGAS-STING pathway is critical for the recognition of DNA viruses and tumors and initiation of the subsequent immune response. Although STING activation leads to multiple outcomes such as proinflammatory cytokine production and autophagy, most studies on STING-related diseases have focused on type I IFN production as the major downstream player. In order to dissect the role of distinct STING signaling functions in vivo, we generated three different STING mutant mice: S365A, L373A, and ΔCTT. Here, we show that STING-S365A mutant mice that lost type I IFN induction are still resistant to HSV-1 infection and can still mount an antitumor response after cGAMP treatment, suggesting an IFN-independent antiviral and antitumor effect mediated by STING. Such an effect was not observed in STING-L373A that failed to recruit TBK1, indicating STING mediates antiviral and antitumor functions through a mechanism that depends on TBK1 recruitment but is independent of type I IFN induction. Since the STING-L373A mutant induces autophagy normally, the results also suggest that STING-induced autophagy is not sufficient to drive an antiviral or antitumor response in vivo.

Two recent papers reported that STING-S365A mice were resistant to HSV-1 infection (30, 31), similar to our results. In one of the studies, it was suggested that STING-induced, TBK1-dependent autophagy explains this effect as TBK1 was required for this antiviral effect and STING-ΔCTT mice, which lost autophagy induction, were susceptible to HSV-1 infection (31). However, our study provides another STING mutant model, L373A, that lost TBK1/IKKε activation but retained autophagy induction. We showed that STING-L373A mice were susceptible to HSV-1 infection, indicating that autophagy alone is not sufficient to drive the antiviral response by STING in vivo (Fig. 2*A*). Our data confirm that TBK1 is dispensable for STING-induced LC3 lipidation in primary cells (Fig. 1*A*), which was previously only described in mammalian cell lines (6, 7). However, our result does not determine if STING-induced autophagy is essential for restricting HSV-1 in vivo; such analysis would require a STING autophagy-specific mutation, which has yet to be discovered. Nevertheless, inflammation and immune cells activated by TBK1 recruitment to STING may play a more critical role in vivo to restrict viral infections. The NF-κB pathway is a strong candidate for the IFN-independent STING-induced antiviral responses. We showed that NF-κB–driven genes such as CXCL1, CXCL2, and 4-1BBL are up-regulated in STING-S365A cells that may contribute to viral resistance (Fig. 4). Monocytes and neutrophils were previously reported to restrict the replication and spread of HSV (37–39); CXCL1 and CXCL2 may exert an antiviral function by recruiting monocytes and neutrophils to the infected site. 4-1BBL was shown to expand lymphocytic choriomeningitis

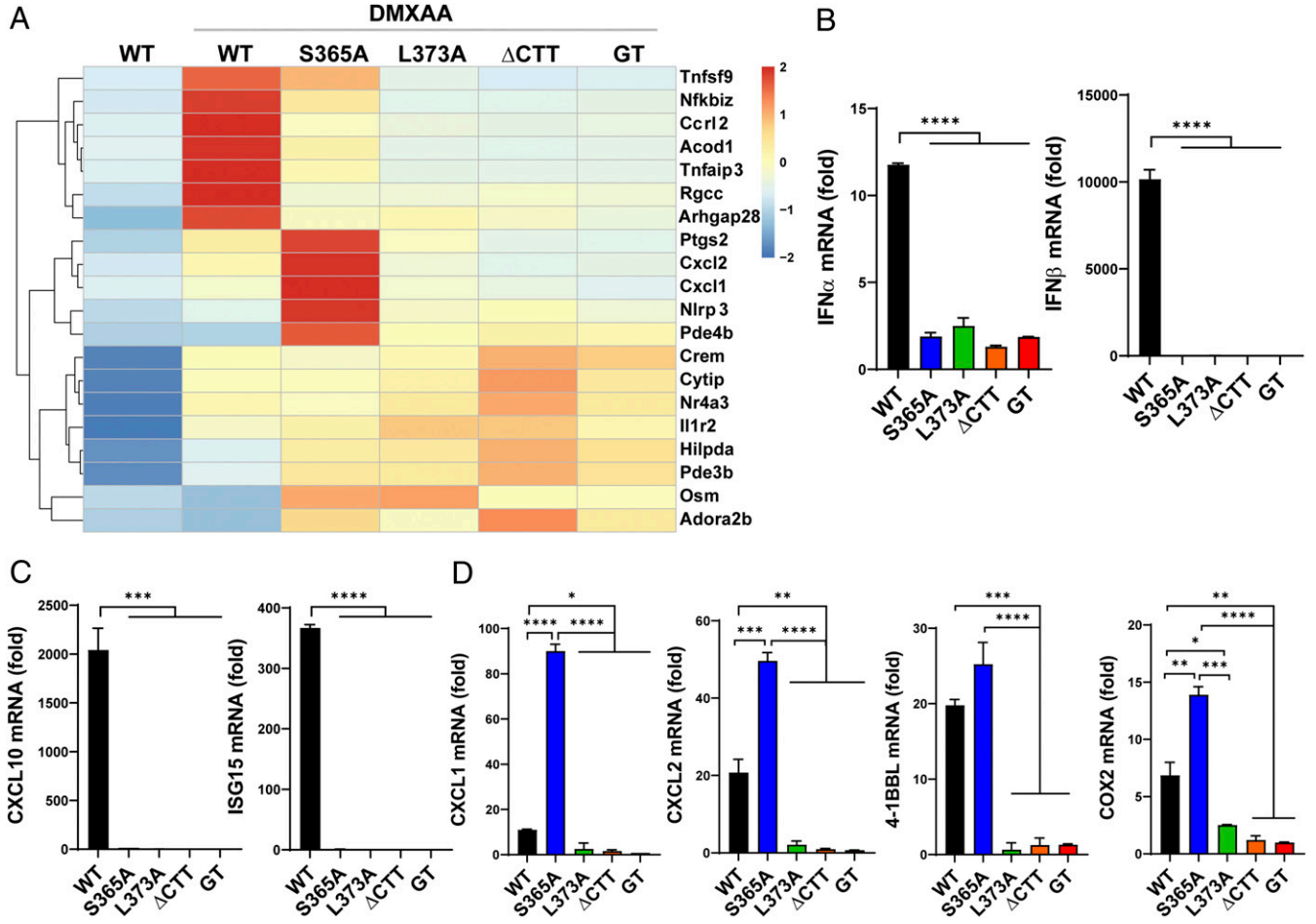

Fig. 4. Transcriptome analysis of STING-regulated genes in primary cells from STING mutant mice. (*A*) Heatmap showing the top 20 genes up-regulated in DMXAA-treated STING-S365A BMDMs relative to untreated WT cells. RNA was extracted from BMDMs treated with 75 μM DMXAA for 2 h. (*B–D*) qRT-PCR analysis of BMDCs treated with 75 μM DMXAA for 2 h. As baseline expression levels were comparable among untreated STING mutant cells, expression levels were normalized by untreated WT cells. (*B*) IFNα and IFNβ. (*C*) Interferon-stimulated genes. (*D*) Genes expressed highly in STING-S365A BMDCs. Error bars represent SEM. $^*P < 0.05$, $^{**}P < 0.01$, $^{***}P < 0.001$, $^{****}P < 0.0001$. mRNA, messenger RNA.

virus-specific $CD8^+$ T cells and thus may contribute to T cell-mediated antiviral immunity (40). Further studies are needed to determine whether the STING-induced NF-κB signaling or other pathways elicited by STING play a major role in defending against pathogen infections in the absence of STING-induced type I IFNs.

The specific role of type I IFNs in the antiviral response also requires further study. STING mutant mice that lack STING-induced type I IFN production survived HSV-1 infection (Fig. 2*A*) (30, 31) while IFNAR-deficient mice were highly susceptible to HSV-1 infection (22). These results suggest that STING-independent IFN production in response to HSV-1 infection is necessary for the antiviral response (41). TLR2, TLR3, and TLR9 have been reported to detect HSV-1 and induce type I IFNs (42–44). In the absence of STING-induced IFNs, these pathways may compensate for defective STING signaling and play a vital role in antiviral immunity. Indeed, we observed comparable levels of serum IFNβ in WT and all STING mutant mice 2 d postinfection (*SI Appendix*, Fig. S2*B*). Which pathway produces this type I IFN and how this later IFN production provides an antiviral effect need to be investigated further. Nevertheless, the cGAS-STING pathway is responsible for the rapid initial IFN response after infection (Fig. 2*B*). Moreover, since the STING-L373A mutant mice are completely susceptible to HSV-1 infection, the IFN-independent immune defense functions of STING cannot be compensated by another pathway.

Our study revealed that STING activation provides a potent antitumor effect against LL2 through both a type I IFN-dependent and -independent mechanism. Based on the significant antitumor effect by cGAMP in STING-S365A mice, but not in -L373A mice, the NF-κB pathway is suggested as the main candidate for providing this antitumor effect. NF-κB signaling and the subsequent inflammation are known to induce both antitumor and protumor responses. Chronic and persistent low-level inflammation recruits suppressive immune cells such as regulatory T cells and myeloid-derived suppressor cells, which inhibit antitumor immune responses; NF-κB signaling also promotes metastasis by inducing cancer cell proliferation and angiogenesis (45). Chronic activation of STING by tumors was also implicated in promoting tumor metastasis (29, 46). However, acute activation of the NF-κB pathway promotes perforin and IFNγ expression by NK cells (47, 48). In addition, NF-κB in $CD4^+$ T cells was essential to reject fibrosarcoma tumors and to activate tumor-specific T cells (49). We observed activation of innate and adaptive immune cells by STING in an IFN-independent manner in vitro (Fig. 5*B*). In the LL2 tumor model, the antitumor effect of cGAMP was partially dependent on NK cells (*SI Appendix*, Fig. S5*H*). In this regard, interaction of 4-1BB on NK cells with 4-1BBL–expressing cells promoted NK cell proliferation, and the agonistic anti–4-1BB has shown an NK cell-dependent antitumor effect on mastocytoma (50, 51). cGAMP treatment

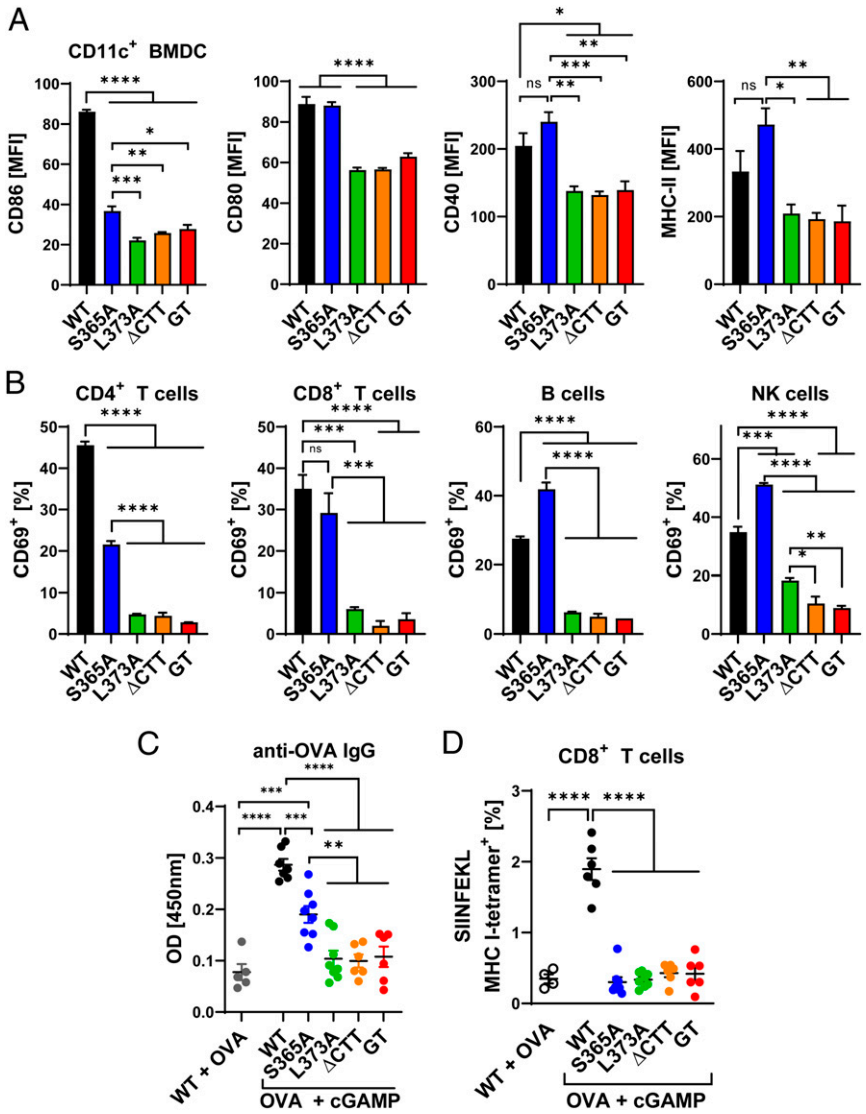

Fig. 5. IFN-independent functions of STING have immunostimulatory effects. (*A*) BMDCs were stimulated with 75 μM DMXAA for 22 h, and $CD11c^+$ cells were analyzed by flow cytometry with antibodies against the indicated proteins. MFI, mean fluorescence intensity. (*B*) Splenocytes were stimulated with 37.5 μM DMXAA for 18 h, and $CD4^+$ T cells ($CD3^+$ $CD4^+$), $CD8^+$ T cells ($CD3^+$ $CD8^+$), B cells ($CD3^-$ $B220^+$), and NK cells ($CD3^-$ $NK1.1^+$) were analyzed by flow cytometry using CD69 as the activation marker. (*C*) Mice were intramuscularly injected with 50 μg of OVA with or without 10 μg of cGAMP on days 0 and 7; sera and splenocytes were collected on day 14. (*C*) Serum ELISA for anti-OVA IgG. (*D*) Flow cytometric analysis of OVA-specific $CD8^+$ T cells stained with tetramers. Error bars represent SEM. $*P < 0.05$, $**P < 0.01$, $***P < 0.001$, $****P < 0.0001$. Results are representative of at least two independent experiments.

recruited $Ly6G^+$ neutrophil-like cells into the tumor (*SI Appendix*, Fig. S5*E*) and induced NOS2 (N1 phenotype) while down-regulating ARG1 (N2 phenotype) in the tumor (*SI Appendix*, Fig. S5*F*). N1 neutrophils have the potential to direct tumor cell death through the production of reactive oxygen species (36). Mechanistically, reactive oxygen species acted on the H_2O_2-dependent calcium channel TRPM2 on cancer cells, including LL2 cells, to mediate lethal influx of calcium ions (52). Moreover, depleting neutrophils in mice reduced the antitumor effect of radiation therapy (53), which is known to activate the cGAS-STING pathway (54). As STING-S365A cells induce the neutrophil chemoattractants CXCL1 and CXCL2 upon stimulation, neutrophils may contribute to the type I IFN-independent antitumor effect. Further studies are needed to determine how STING-induced NF-κB signaling drives this IFN-independent immunostimulatory effect and the subsequent antiviral and antitumor response.

The CTT of STING was dispensable for autophagy induction in stable cell lines (6) but the LC3 lipidation was weaker in BMDCs derived from the STING-ΔCTT mice (Fig. 1*A*), potentially due to the lower levels of native expression of STING-ΔCTT. We observed a stronger induction of NF-κB–induced genes in STING-S365A cells compared with WT cells (Fig. 4), suggesting that STING-induced IRF3 activation may inhibit NF-κB–induced gene expression. IRF3 and NF-κB synergistically induce type I IFNs, but the regulatory cross-talk between STING-induced IRF3 and NF-κB has not been well-studied. A previous study found that IFNα pretreatment in BMDMs inhibits CXCL1 and CXCL2 induction by a TLR2 ligand (55). In addition, $IRF3^{-/-}$ $IRF7^{-/-}$ mice showed higher CXCL1 and CXCL2 expression in influenza A-infected lungs (56). We observed increased expression of several NF-κB–induced genes in STING-S365A cells, further supporting such regulatory cross-talk between the NF-κB pathway and the IFN pathway.

In summary, our study has demonstrated the type I IFN-independent antiviral and antitumor immune defense that is mediated by TBK1 recruitment to STING. Activation of the immune system by STING is critical for fighting cancer and infectious diseases, but can also lead to autoimmunity (57). Interestingly, murine models of autoimmune disease with overactive STING signaling developed inflammation even in the absence of IRF3 or IFNAR (58, 59). Further studies on the type I IFN-independent role of STING in immune-related diseases will provide new insights into the physiological and pathological functions of STING, which are important for developing safe and effective treatments for human diseases.

Materials and Methods

Mice. All mice used in this study were on the C57BL/6 background. Male mice were used for HSV-1 experiments, and female mice were used for tumor experiments. STING-S365A, -L373A, and -ΔCTT mice were generated using the CRISPR-Cas9 system. CRISPR RNAs and template DNA oligos were purchased from Integrated DNA Technologies (*SI Appendix*, Table S1). In vitro fertilization was done by the University of Texas (UT) Southwestern Transgenic Technology Center. WT and Sting^{gt} mice were purchased from The Jackson Laboratory. *Ifnb1*$^{\Delta\beta\text{-luc}/\Delta\beta\text{-luc}}$ mice were provided by Rayk Behrendt, University of Technology, Dresden, Germany (60) and crossed with the *Cgas*$^{-/-}$ mice generated in our laboratory (19). *Ifnar1*$^{-/-}$ mice were provided by David Farrar, UT Southwestern. Mice were bred and maintained under specific pathogen-free conditions in the animal facility of the University of Texas Southwestern Medical Center at Dallas according to experimental protocols approved by the Institutional Animal Care and Use Committee.

Primary Cells. Splenocytes or bone marrow cells were filtered through a 70-μm strainer and treated with Red Blood Cell Lysis Buffer (Sigma). For generation of BMDMs, bone marrow cells were cultured in 15 ng/mL macrophage colony-stimulating factor (PeproTech) and 20% fetal bovine serum (FBS) in complete Dulbecco's modified Eagle's medium (DMEM) for 7 d; the medium was replenished on days 3 and 6. For BMDCs, bone marrow cells were cultured in 10 ng/mL granulocyte-macrophage colony-stimulating factor (PeproTech) and 10% FBS in Complete RPMI 1640 Medium for 6 d; the medium was replenished on days 3 and 5. These cells were treated with 75 μM DMXAA (Sigma) unless otherwise indicated.

HSV-1 Experiments. HSV-1 and HSV-1-GFP were propagated and titered by plaque assays on Vero cells (19). Male mice were infected with HSV-1 (5×10^6 plaque-forming units per mouse) retroorbitally under isoflurane anesthesia. For viral titer measurements, Vero cells were incubated with mouse brain homogenates at serial dilutions for 1 h and then overlaid with 1.5% methylcellulose in DMEM containing 1% FBS. Seventy-two hours later, cells were fixed in methanol and formaldehyde and stained with 0.1% crystal violet. Plaques were counted to calculate viral titer from the inoculum and dilutions. For in vitro infections, cells were infected with the indicated multiplicity of infection of HSV-1 or HSV-1-GFP. DNA from HSV-1–infected cells was isolated using the DNeasy Blood & Tissue Kit (Qiagen), and the VGE was measured by qPCR and normalized by adipsin (61). HSV-1-GFP–infected cells were analyzed by flow cytometry.

LL2 Tumor Experiments. LL2 tumor cells were grown in complete DMEM. LL2 cells (1×10^6) were subcutaneously injected into the flank of mice. Mice were intratumorally treated with 10 μg of cGAMP unless otherwise indicated. InVivoMab was purchased from Bio X Cell; anti-mouse PD-L1, anti-CD8α, and anti-NK1.1 were injected intraperitoneally, and anti-mouse IFNAR-1 was injected intratumorally. Tumor sizes were measured every 2 or 3 d and calculated by (length × width × height × 3.14)/6. For the IFNβ promoter-driven luciferase activity, LL2-implanted *Ifnb1*$^{\Delta\beta\text{-luc}/\Delta\beta\text{-luc}}$ mice were intraperitoneally injected with 3 mg of VivoGlo luciferin (Promega) in phosphate-buffered saline (PBS). Photon flux from mice was measured by an IVIS Lumina under isoflurane anesthesia. For tumor-infiltrating immune cell analyses, LL2 tumors were digested in 1 mg/mL collagenase A and 20 μg/mL DNase I (Roche) for 30 min at 37 °C before filtering through 100-μm cell strainers (Greiner Bio-One).

Immunoblotting and Immunostaining. For immunoblotting, cells were lysed in 2× sample buffer, separated by sodium dodecyl sulfate-polyacrylamide gel electrophoresis (Bio-Rad), and blotted with primary antibodies followed by horseradish peroxidase (HRP)-conjugated secondary antibodies (Cell Signaling). For immunostaining, cells were fixed with 4% paraformaldehyde, permeabilized with 0.1% Triton X-100, and stained with primary antibodies, followed by Alexa 488-conjugated secondary antibody (Invitrogen). Coverslips were coated with 50 μg/mL poly-D-lysine (Sigma) to adhere BMDCs. Stained slides were mounted on DAPI-mounting media (Vectashield) and analyzed with an LSM700 confocal microscope. Antibodies against p-STING (S365), p-IRF3 (S396), p-IκBα (S32), p-TBK1 (S172), p-STAT1 (Y701), p-NF-κB p65 (S536), p-IKKε (S172), LC3A/B, and GAPDH were from Cell Signaling; anti-mouse STING was from Proteintech; and anti–α-tubulin was from Sigma.

Flow Cytometry and ELISA. Cells were stained with fluorophore-labeled antibodies and fixed with 4% paraformaldehyde before analysis with a BD FACSCalibur or LSRII. The following antibodies from BioLegend were used for flow cytometry: CD45-A700, CD69-FITC/-PB, CD80-FITC, NK1.1-PE, CD11b-FITC, CD11c-PE, B220-PerCP-Cy5.5, I-A/I-E-PerCP-Cy5.5, Ly6G-PE, Ly6C-APC, CD3-APC/-FITC, CD40-APC, PD-L1-APC, IgG2b-κ-APC, CD45-A700, CD4-APC/-PB, CD86-PB, and CD8-PerCP-Cy5.5/-BV711. APC-labeled H-2K(b) SIINFEKL tetramer was from the NIH. IFNβ levels in cell-culture media and mouse sera were measured with an IFNβ enzyme-linked immunosorbent assay (ELISA) kit (Invivogen) according to the manufacturer's instructions. For anti-OVA IgG ELISA, 96-well ELISA plates (Greiner Bio-One) were coated with 10 μg/mL of OVA (Sigma) and incubated with diluted sera. These plates were incubated with HRP-conjugated anti-mouse IgG (Cell Signaling), and the optical density (OD) at 450 nm was measured after developing with 3,3′,5,5′-tetramethylbenzidine substrate (Thermo Scientific).

RNA Sequencing. RNA was isolated using an RNeasy Mini Kit (Qiagen) and sequenced by Novogene. All analysis was conducted in R (version 4.0.2). For DEG (differentially expressed gene) analysis, we used the R package edgeR and followed the user guide (62, 63). Genes with adjusted P value < 0.05 (adjusted using Benjamini–Hochberg methods) were considered as significant DEGs. The FPKM (fragments per kilobase of transcript per million mapped reads) value of each gene was generated using the R package countToFPKM. The gene expression heatmap was plotted using the R package Pheatmap with the FPKM of each gene as an input. The KEGG pathway enrichment analysis was done using the R package clusterProfiler (64). Significantly enriched pathways were selected based on an adjusted P value < 0.05. Bar plots were generated using the R package ggplot2.

qRT-PCR. RNA was isolated from cells or homogenized tissue using TRIzol Reagent (Invitrogen). The complementary DNA reverse-transcription kit and SYBR Green Master Mix from Applied Biosystems were used for qRT-PCR analysis according to the manufacturer's instructions. Primers used for qRT-PCR are listed in *SI Appendix*, Table S2.

Statistics. Statistical analysis of mouse survival was performed using the Mantel–Cox test. Mouse brain viral titer was analyzed using the Kruskal–Wallis test. Other statistical analyses were performed by one-way ANOVA.

Data Availability. All study data are included in the article and/or *SI Appendix*.

ACKNOWLEDGMENTS. We thank Dr. Rayk Behrendt for providing the *Ifnb1*$^{\Delta\beta\text{-luc}/\Delta\beta\text{-luc}}$ mice and Yafang Deng for generating the LL2-STING$^{-/-}$ cells. M.L. was supported by the National Institute of Allergy and Infectious Diseases of the NIH (T32AI005284). This work was supported by grants from the National Cancer Institute (U54CA244719), Welch Foundation (I-1389), and Cancer Prevention and Research Institute of Texas (RP180725). Z.J.C. is an Investigator of the Howard Hughes Medical Institute.

1. H. Ishikawa, G. N. Barber, STING is an endoplasmic reticulum adaptor that facilitates innate immune signalling. *Nature* **455**, 674–678 (2008).
2. B. Zhong *et al.*, The adaptor protein MITA links virus-sensing receptors to IRF3 transcription factor activation. *Immunity* **29**, 538–550 (2008).
3. W. Sun *et al.*, ERIS, an endoplasmic reticulum IFN stimulator, activates innate immune signaling through dimerization. *Proc. Natl. Acad. Sci. U.S.A.* **106**, 8653–8658 (2009).
4. L. Sun, J. Wu, F. Du, X. Chen, Z. J. Chen, Cyclic GMP-AMP synthase is a cytosolic DNA sensor that activates the type I interferon pathway. *Science* **339**, 786–791 (2013).
5. J. Wu *et al.*, Cyclic GMP-AMP is an endogenous second messenger in innate immune signaling by cytosolic DNA. *Science* **339**, 826–830 (2013).
6. X. Gui *et al.*, Autophagy induction via STING trafficking is a primordial function of the cGAS pathway. *Nature* **567**, 262–266 (2019).

7. D. Liu *et al*., STING directly activates autophagy to tune the innate immune response. *Cell Death Differ.* **26**, 1735–1749 (2019).
8. C. Zhang *et al*., Structural basis of STING binding with and phosphorylation by TBK1. *Nature* **567**, 394–398 (2019).
9. Y. Tanaka, Z. J. Chen, STING specifies IRF3 phosphorylation by TBK1 in the cytosolic DNA signaling pathway. *Sci. Signal.* **5**, ra20 (2012).
10. S. Liu *et al*., Phosphorylation of innate immune adaptor proteins MAVS, STING, and TRIF induces IRF3 activation. *Science* **347**, aaa2630 (2015).
11. T. Abe, G. N. Barber, Cytosolic-DNA-mediated, STING-dependent proinflammatory gene induction necessitates canonical NF-κB activation through TBK1. *J. Virol.* **88**, 5328–5341 (2014).
12. K. R. Balka *et al*., TBK1 and IKKε act redundantly to mediate STING-induced NF-κB responses in myeloid cells. *Cell Rep.* **31**, 107492 (2020).
13. S. T. Smale, Selective transcription in response to an inflammatory stimulus. *Cell* **140**, 833–844 (2010).
14. B. W. Davies, R. W. Bogard, T. S. Young, J. J. Mekalanos, Coordinated regulation of accessory genetic elements produces cyclic di-nucleotides for *V. cholerae* virulence. *Cell* **149**, 358–370 (2012).
15. G. B. Severin *et al*., Direct activation of a phospholipase by cyclic GMP-AMP in El Tor *Vibrio cholerae*. *Proc. Natl. Acad. Sci. U.S.A.* **115**, E6048–E6055 (2018).
16. D. Cohen *et al*., Cyclic GMP-AMP signalling protects bacteria against viral infection. *Nature* **574**, 691–695 (2019).
17. Y. Liu *et al*., Inflammation-induced, STING-dependent autophagy restricts Zika virus infection in the *Drosophila* brain. *Cell Host Microbe* **24**, 57–68.e3 (2018).
18. M. Martin, A. Hiroyasu, R. M. Guzman, S. A. Roberts, A. G. Goodman, Analysis of *Drosophila* STING reveals an evolutionarily conserved antimicrobial function. *Cell Rep.* **23**, 3537–3550.e6 (2018).
19. X. D. Li *et al*., Pivotal roles of cGAS-cGAMP signaling in antiviral defense and immune adjuvant effects. *Science* **341**, 1390–1394 (2013).
20. H. Ishikawa, Z. Ma, G. N. Barber, STING regulates intracellular DNA-mediated, type I interferon-dependent innate immunity. *Nature* **461**, 788–792 (2009).
21. L. S. Reinert *et al*., Sensing of HSV-1 by the cGAS-STING pathway in microglia orchestrates antiviral defence in the CNS. *Nat. Commun.* **7**, 13348 (2016).
22. D. A. Leib *et al*., Interferons regulate the phenotype of wild-type and mutant herpes simplex viruses in vivo. *J. Exp. Med.* **189**, 663–672 (1999).
23. L. S. Reinert *et al*., TLR3 deficiency renders astrocytes permissive to herpes simplex virus infection and facilitates establishment of CNS infection in mice. *J. Clin. Invest.* **122**, 1368–1376 (2012).
24. S. R. Woo *et al*., STING-dependent cytosolic DNA sensing mediates innate immune recognition of immunogenic tumors. *Immunity* **41**, 830–842 (2014).
25. S. Yum, M. Li, A. E. Frankel, Z. J. Chen, Roles of the cGAS-STING pathway in cancer immunosurveillance and immunotherapy. *Annu. Rev. Cancer Biol.* **3**, 323–344 (2019).
26. L. Corrales *et al*., Direct activation of STING in the tumor microenvironment leads to potent and systemic tumor regression and immunity. *Cell Rep.* **11**, 1018–1030 (2015).
27. O. Demaria *et al*., STING activation of tumor endothelial cells initiates spontaneous and therapeutic antitumor immunity. *Proc. Natl. Acad. Sci. U.S.A.* **112**, 15408–15413 (2015).
28. Y. Hou *et al*., Non-canonical NF-κB antagonizes STING sensor-mediated DNA sensing in radiotherapy. *Immunity* **49**, 490–503.e4 (2018).
29. S. F. Bakhoum *et al*., Chromosomal instability drives metastasis through a cytosolic DNA response. *Nature* **553**, 467–472 (2018).
30. J. Wu, N. Dobbs, K. Yang, N. Yan, Interferon-independent activities of mammalian STING mediate antiviral response and tumor immune evasion. *Immunity* **53**, 115–126.e5 (2020).
31. L. H. Yamashiro *et al*., Interferon-independent STING signaling promotes resistance to HSV-1 in vivo. *Nat. Commun.* **11**, 3382 (2020).
32. J. D. Sauer *et al*., The *N*-ethyl-*N*-nitrosourea-induced Goldenticket mouse mutant reveals an essential function of Sting in the in vivo interferon response to *Listeria monocytogenes* and cyclic dinucleotides. *Infect. Immun.* **79**, 688–694 (2011).
33. H. Wang *et al*., cGAS is essential for the antitumor effect of immune checkpoint blockade. *Proc. Natl. Acad. Sci. U.S.A.* **114**, 1637–1642 (2017).
34. S. Lienenklaus *et al*., Novel reporter mouse reveals constitutive and inflammatory expression of IFN-beta in vivo. *J. Immunol.* **183**, 3229–3236 (2009).
35. H. Y. Li *et al*., The tumor microenvironment regulates sensitivity of murine lung tumors to PD-1/PD-L1 antibody blockade. *Cancer Immunol. Res.* **5**, 767–777 (2017).
36. M. A. Giese, L. E. Hind, A. Huttenlocher, Neutrophil plasticity in the tumor microenvironment. *Blood* **133**, 2159–2167 (2019).
37. T. M. Tumpey, S. H. Chen, J. E. Oakes, R. N. Lausch, Neutrophil-mediated suppression of virus replication after herpes simplex virus type 1 infection of the murine cornea. *J. Virol.* **70**, 898–904 (1996).
38. G. N. Milligan, Neutrophils aid in protection of the vaginal mucosae of immune mice against challenge with herpes simplex virus type 2. *J. Virol.* **73**, 6380–6386 (1999).
39. N. Iijima, L. M. Mattei, A. Iwasaki, Recruited inflammatory monocytes stimulate antiviral Th1 immunity in infected tissue. *Proc. Natl. Acad. Sci. U.S.A.* **108**, 284–289 (2011).
40. J. T. Tan, J. K. Whitmire, R. Ahmed, T. C. Pearson, C. P. Larsen, 4-1BB ligand, a member of the TNF family, is important for the generation of antiviral CD8 T cell responses. *J. Immunol.* **163**, 4859–4868 (1999).
41. S. R. Paludan, A. G. Bowie, K. A. Horan, K. A. Fitzgerald, Recognition of herpesviruses by the innate immune system. *Nat. Rev. Immunol.* **11**, 143–154 (2011).
42. H. Hochrein *et al*., Herpes simplex virus type-1 induces IFN-alpha production via Toll-like receptor 9-dependent and -independent pathways. *Proc. Natl. Acad. Sci. U.S.A.* **101**, 11416–11421 (2004).
43. A. Krug *et al*., Herpes simplex virus type 1 activates murine natural interferon-producing cells through Toll-like receptor 9. *Blood* **103**, 1433–1437 (2004).
44. L. N. Sørensen *et al*., TLR2 and TLR9 synergistically control herpes simplex virus infection in the brain. *J. Immunol.* **181**, 8604–8612 (2008).
45. K. Taniguchi, M. Karin, NF-κB, inflammation, immunity and cancer: Coming of age. *Nat. Rev. Immunol.* **18**, 309–324 (2018).
46. Q. Chen *et al*., Carcinoma-astrocyte gap junctions promote brain metastasis by cGAMP transfer. *Nature* **533**, 493–498 (2016).
47. J. Zhou, J. Zhang, M. G. Lichtenheld, G. G. Meadows, A role for NF-kappa B activation in perforin expression of NK cells upon IL-2 receptor signaling. *J. Immunol.* **169**, 1319–1325 (2002).
48. C. M. Tato *et al*., Opposing roles of NF-kappaB family members in the regulation of NK cell proliferation and production of IFN-gamma. *Int. Immunol.* **18**, 505–513 (2006).
49. S. E. Barnes *et al*., T cell-NF-κB activation is required for tumor control in vivo. *J. Immunother. Cancer* **3**, 1 (2015).
50. I. Barao, The TNF receptor-ligands 4-1BB-4-1BBL and GITR-GITRL in NK cell responses. *Front. Immunol.* **3**, 402 (2013).
51. D. S. Vinay, B. S. Kwon, Immunotherapy of cancer with 4-1BB. *Mol. Cancer Ther.* **11**, 1062–1070 (2012).
52. M. Gershkovitz *et al*., TRPM2 mediates neutrophil killing of disseminated tumor cells. *Cancer Res.* **78**, 2680–2690 (2018).
53. T. Takeshima *et al*., Key role for neutrophils in radiation-induced antitumor immune responses: Potentiation with G-CSF. *Proc. Natl. Acad. Sci. U.S.A.* **113**, 11300–11305 (2016).
54. L. Deng *et al*., STING-dependent cytosolic DNA sensing promotes radiation-induced type I interferon-dependent antitumor immunity in immunogenic tumors. *Immunity* **41**, 843–852 (2014).
55. A. Shahangian *et al*., Type I IFNs mediate development of postinfluenza bacterial pneumonia in mice. *J. Clin. Invest.* **119**, 1910–1920 (2009).
56. B. Hatesuer *et al*., Deletion of Irf3 and Irf7 genes in mice results in altered interferon pathway activation and granulocyte-dominated inflammatory responses to influenza A infection. *J. Innate Immun.* **9**, 145–161 (2017).
57. Y. J. Crow, N. Manel, Aicardi-Goutières syndrome and the type I interferonopathies. *Nat. Rev. Immunol.* **15**, 429–440 (2015).
58. J. D. Warner *et al*., STING-associated vasculopathy develops independently of IRF3 in mice. *J. Exp. Med.* **214**, 3279–3292 (2017).
59. K. Kawane *et al*., Chronic polyarthritis caused by mammalian DNA that escapes from degradation in macrophages. *Nature* **443**, 998–1002 (2006).
60. K. Peschke *et al*., Loss of Trex1 in dendritic cells is sufficient to trigger systemic autoimmunity. *J. Immunol.* **197**, 2157–2166 (2016).
61. J. P. Katz, E. T. Bodin, D. M. Coen, Quantitative polymerase chain reaction analysis of herpes simplex virus DNA in ganglia of mice infected with replication-incompetent mutants. *J. Virol.* **64**, 4288–4295 (1990).
62. M. D. Robinson, D. J. McCarthy, G. K. Smyth, edgeR: A Bioconductor package for differential expression analysis of digital gene expression data. *Bioinformatics* **26**, 139–140 (2010).
63. D. J. McCarthy, Y. Chen, G. K. Smyth, Differential expression analysis of multifactor RNA-seq experiments with respect to biological variation. *Nucleic Acids Res.* **40**, 4288–4297 (2012).
64. G. Yu, L. G. Wang, Y. Han, Q. Y. He, clusterProfiler: An R package for comparing biological themes among gene clusters. *OMICS* **16**, 284–287 (2012).